Optimizing Receiver Configurations for Resolution of Equivalent Dipole Polarizabilities In Situ

J Torquil Smith, H Frank Morrison
Lawrence Berkeley National Laboratory
Berkeley, California 94720

ABSTRACT

Equivalent dipole polarizabilities are a succinct way to summarize the inductive response of an isolated conductive body at distances greater than the scale of the body. At any time lag or frequency, an equivalent dipole polarizability response is comprised of 9 parameters; six specifying an equivalent dipole polarizability matrix (which is symmetric) and three specifying the apparent location of the body center. Smith and Morrison (2002) give equations for calculating uncertainties in equivalent dipole polarizability and position based on analysis of an iterative linearized inversion.

Here, the root mean squared uncertainty in polarizability is weighted and summed over a number of control points and minimized using an evolutionary algorithm for a number of instrument designs. Three families of designs are presented: single transmitter systems for use on a 2-D grid of positions with negligible error in relative instrument location, two transmitter systems for use on a line of positions with negligible error in relative instrument location, and three transmitter systems for stand alone use. Results for the one and two transmitter systems are strongly degraded by errors in instrument position, whereas the three transmitter systems are insensitive to instrument positioning errors.

INTRODUCTION

Equivalent dipoles have long been used for approximating potential fields in geophysics as well other fields, and we will not attempt to outline the history of their usage. Recently, they have been used to model secondary magnetic fields arising from currents induced in isolated conductive, and possibly magnetic bodies, for discrimination between unexploded ordnance (UXO) and other materials, for example, by Khadr *et al.* (1998), Bell *et al.* (2001), Pasion and Oldenburg (2001), Smith and Morrison (2002) or Baum (1999). In these examples, the induced dipoles are modelled as linearly proportional to the inducing magnetic fields at the body centers. Since the inducing magnetic fields are, in general, vector, and the induced dipoles may have components in x, y and z directions, the two are related by a matrix. Letting $\mathbf{B}^{(s)}(\mathbf{r},t)$ be the secondary magnetic fields due to currents induced in a body by a primary inducing field of nominal strength $\mathbf{B}^{(o)}$ at the center of the body (as it would be in the absence of the body), and letting $\mathbf{B}_x^{(d)}(\mathbf{r})$, $\mathbf{B}_y^{(d)}(\mathbf{r})$, and $\mathbf{B}_z^{(d)}(\mathbf{r})$, be the fields of unit magnetic dipoles in the **x**, **y**, and **z** direction placed at the body center, then an equivalent dipole polarizability representation of the field approximates the field as

$$\mathbf{B}^{(s)}(\mathbf{r},t) \;=\; \left(\mathbf{B}_x^{(d)}(\mathbf{r}), \mathbf{B}_y^{(d)}(\mathbf{r}), \mathbf{B}_z^{(d)}(\mathbf{r})\right)\; \mathbf{M}(t)\; \mathbf{B}^{(o)}\;, \tag{1}$$

where

$$\mathbf{M}(t) \;\equiv\; \begin{pmatrix} m_{xx} & m_{xy} & m_{xz} \\ m_{yx} & m_{yy} & m_{yz} \\ m_{zx} & m_{zy} & m_{zz} \end{pmatrix}\;, \tag{2}$$

is the equivalent dipole polarizability matrix and is 3 x 3 and symmetric, with dimensions of magnetic moment per magnetic induction. In time domain applications, typically, the fields are observed after the primary magnetic fields due to currents in a transmitter coil are extinguished, so the entire measured fields are secondary fields $\mathbf{B}^{(s)}$. In practice, the position of the center of the body is generally not known, and the origin of equivalent dipole fields $\mathbf{r}_o$ is fit to a set of data, yielding an effective object center which may be displaced from the geometric center of the object. Since the polarizability matrix contains information about secondary magnetic fields for any orientation of primary magnetic field $\mathbf{B}_o$, secondary magnetic field field measurements from sources with primary fields in at least three different (linearly independent) directions at the body center are needed to estimate the polarizability matrix.

Assuming that the effective object center is independent of time of field measurement after transmitter shut-off, differentiating equation (1) gives

$$d\mathbf{B}^{(s)}(\mathbf{r},t)\,/\,dt \;=$$

$$\left(\mathbf{B}_x^{(d)}(\mathbf{r}), \mathbf{B}_y^{(d)}(\mathbf{r}), \mathbf{B}_z^{(d)}(\mathbf{r})\right) \; d\mathbf{M}(t)/dt \; \mathbf{B}^{(o)} \quad , \quad (3)$$

where the polarizability change rate $d\mathbf{M}(t)/dt$ is frequently also referred to as the polarizability matrix.

In frequency domain applications, the same equations apply, with t replaced with ω, but $\mathbf{M}(\omega)$ is in general complex (and symmetric), and the secondary fields must be separated from the primary fields of the inducing sources.

The eigenvectors of $\mathbf{M}$ (or $d\mathbf{M}/dt$) give an empirical set of principal directions for an object. For an object with an axis of symmetry, the symmetry implies that two eigenvalues are identical, and that the eigenvector corresponding to the remaining eigenvalue is parallel to the axis of symmetry. For objects with spherical symmetry the three eigenvalues are identical. The eigenvalues of $\mathbf{M}$ or $d\mathbf{M}/dt$ as a function of time after transmitter current shut off for a given transmitter wave form form the basis of many identification schemes, such as that of Pasion and Oldenberg (2001).

Smith and Morrison (2002) discuss fitting polarizability matrices and equivalent dipole positions to data in detail. In an analysis of an iterative linearized inversion for the non-redundant polarizability matrix elements m_{11}, m_{22}, m_{33}, m_{12}, m_{23}, and m_{13}, and changes Δx_o, Δy_o, Δz_o to a previous estimate of equivalent dipole position $\mathbf{r}_o^{(q)}$, from n measurements of secondary magnetic field components with at least three different primary magnetic field sources or source coil positions, they arrive at equations of the form

$$d_i \; = \; \left(\mathbf{a}_i^{(q)}, \tilde{\mathbf{g}}_i^{(q)}\right) \cdot$$

$$(m_{11},\, m_{22},\, m_{33},\, m_{12},\, m_{23},\, m_{13},\, \Delta x_o,\, \Delta y_o,\, \Delta z_o)^t \quad , \quad (4)$$

for the i'th magnetic field component measurement out of a set of n measurements, on the q'th iteration. Writing equations (4) in matrix form as

$$\mathbf{d} \; = \; \mathbf{F} \cdot \begin{pmatrix} \mathbf{m} \\ \Delta \mathbf{r}_o \end{pmatrix} \quad , \quad (5)$$

and the covariance matrix for the measurement errors in $\mathbf{d}$ as $\mathbf{C}_d$, the squared uncertainties in the polarizabilities (elements of $\mathbf{m}$) and in the components of the equivalent dipole position $\mathbf{r}_o$ lie on the diagonal of

$$cov(\,(\mathbf{m}^t, \mathbf{r}_o^t)\,) \; = \; (\mathbf{F}^t\, \mathbf{C}_d^{-1}\, \mathbf{F})^{-1} \quad . \quad (6)$$

In this paper measurement errors σ_i are approximated as uncorrelated between receivers, so the measurement error covariance matrix $\mathbf{C}_d$ is diagonal with squared measurement errors σ_i^2 on its main diagonal.

Since the structure of equations (1) and (3) is identical, equations of form (4) (and 5) hold when the data is magnetic field data ($\mathbf{B}$) or time derivative data ($d\mathbf{B}/dt$), only in the latter case elements m_{ij} are replaced by their derivatives dm_{ij}/dt in forming equations (4) and (5). The coefficient matrix $\mathbf{F}$ is identical in the two cases. Given identical covariance matrices, the problem of optimizing a receiver array with respect to polarizability uncertainties is identical for the two cases.

Here a number of designs are presented for systems minimizing the squared uncertainty in polarizability weighted and summed for objects at a number of points specified below the system ('control points'). In this paper, instrument systems are comprised of one or several rectangular transmitter loops of fixed size, and a number of receiver coils approximated as point measurements. Three families of designs are presented: systems for use on a 2-D grid of positions with negligible error in relative instrument location, systems for use on a line of positions with negligible error in relative instrument location, and systems for stand alone use, insensitive to instrument positioning errors. The minimizations are made using an empirical distribution evolutionary algorithm.

MINIMIZATION USING AN EMPIRICAL DISTRIBUTION EVOLUTIONARY ALGORITHM

The general problem of minimizing an arbitrary (objective) function of a considerable number of variables remains a difficult problem. One principal difficulty is that the number of sample points required to sample a parameter space uniformly increases as the number of sample points for each parameter raised to the power of the number of variables. Sampling the entire space on a reasonably

detailed grid becomes prohibitively time consuming very quickly. A large number of algorithms have been proposed which result in some initial coarse sampling of the parameter space and later denser resamplings in areas of low objective function. Among these are simulated annealing, evolutionary algorithms, and genetic algorithms. Here we use the empirical distribution evolutionary algorithm of Smith, Allan, and Schultz (1994).

The empirical distribution evolutionary algorithm is a real parameter genetic algorithm with arithmetic recombination, with perturbations to recombined population members based on differences of retained population members and discarded population members. (For an overview of evolutionary algorithms, see, for example, Deb, 2001, pp81-164.) In slightly more detail, to find a minimum of a function of p variables in a bounded domain, the algorithm begins with a sampling of m_{pop} points $\mathbf{x}$, each consisting of p variables distributed (uniformly) throughout bounded intervals. At each iteration, the object function is evaluated at each sample point and a penalty term added to the function at any points that fall outside the desired intervals. The points are divided randomly into m_{save} equal size groups (e.g., $m_{pop}/2$), and the point with the lowest object function (plus penalty term) from each group is collected into a set of m_{save} points $\{\mathbf{x}_{save}\}$ saved for use in the next iteration, the remaining $m_{pop} - m_{save}$ points to be discarded are collected into another set $\{\mathbf{x}_{disc}\}$. At the next iteration, in addition to the saved points, new sample points are formed from the sum of the average of two randomly selected saved points and the difference of one discard point with a randomly selected saved point;

$$\mathbf{x}_{new}^{(k)} \equiv (\mathbf{x}_{save}^{(i)} + \mathbf{x}_{save}^{(j)})/2 \; + \; s_k \alpha \cdot (\mathbf{x}_{disc}^{(k)} - \mathbf{x}_{save}^{(l)}) \, , \tag{7}$$

where $s_k = \pm 1$ with random sign, and $0.59 \leq \alpha$ $1/\sqrt{2}$. Each discard point is used in forming one new sample point. This gives a new point distribution centered at the mean of the saved point distribution. Generally, the new points are closer to the mean of the saved points than the discarded points were, and the cloud of sample points shrinks with iteration. As the algorithm saves the better points from the m_{save} groups, it preserves the best point found at any iteration. Occasionally, the algorithm is caught by distributions straddling widely separated minima. This is dealt with by reducing the number of saved points on a schedule based on the contraction expected for a quadratic object function. As an alternative, when forming the k'th replacement point, after randomly selecting the first saved point $\mathbf{x}_{save}^{(i)}$ used in forming the new sample point, several (m_{suit}) more points are drawn randomly from the set of saved points and the closest of these to the first saved point $\mathbf{x}_{save}^{(i)}$ is used as the second saved point to be averaged $\mathbf{x}_{save}^{(j)}$. In this case, m_{suit} additional saved points are drawn and the closest of these to the discard point is used as $\mathbf{x}_{save}^{(l)}$ in equation (7). In this variant, the amount of perturbation added to the averaged saved points needs to be somewhat larger ($\alpha \geq 0.64$, for $m_{suit} = 3$). Experience has shown this to eliminate the need for progressively reducing the number of saved points m_{save} to escape distributions caught straddling widely separated minima.

One can generally cannot afford to adequately sample all of a parameter space of interest for even moderate p, so guarantees of convergence to the global minimum for adequate sampling by any method are of limited value. For minimizations of objective functions for problems of the sort considered in this paper, we have found the current method to be more reliable than a simple implementation of a simulated annealing method (as per Press *et al.*, 1986). Consequently, all minima presented in this paper correspond to minima as found by the empirical distribution evolutionary algorithm. As the rate of convergence is fairly slow for moderate p due to volume being proportional to p'th power of distance in a p dimensional space, the empirical distribution evolutionary algorithm is used to reduce the difference between the median sample point object function and the lowest value found to a small tolerance and the resulting values improved using the downhill simplex method (Press *et al.*, 1986).

OBJECTIVE FUNCTION

Generally, for polarizability matrix elements m_{ij} to be well determined, the equivalent dipole position $\mathbf{r}_o$ must also be well determined, so we concentrate

on resolving elements m_{ij}. The squared uncertainties in the non-redundant polarizability elements are given by the first six elements on the main diagonal of $cov((\mathbf{m}^t, \mathbf{r}_o^t))$, and are denoted by $var(m_{ij})$ for i and j indexed appropriately. Because of symmetry of $\mathbf{M}$, $m_{ij} = m_{ji}$, consequently $var(m_{ij}) = var(m_{ji})$. For an object at a given position, given its polarizability $\mathbf{M}$ equation (6) allows calculating the squared uncertainties that would be present in estimates of the polarizability elements m_{ij} recovered from inversion of data for any particular system of transmitters and dipole receivers.

Generally, for small objects a given instrument only has sensitivity to objects close to the instrument, so it is futile to demand high precision for objects very distant from the instrument. For small objects closer to a system than the scale of the transmitter loops uncertainty in m_{ij} increases roughly as z^3, approaching a z^6 (or larger) dependence at depths greater than the transmitter loop scale (Smith *et al.*, 2002). Similarly, for ease in deployment (as on a wheeled cart) it is common to allow some clearance between an instrument and the zone containing possible objects (the ground). Defining the total squared polarizability uncertainty for an object at depth z as

$$\varepsilon^2(z_i) \equiv \sum_{i=1}^{3} \sum_{j=1}^{3} var(m_{ij}) \ , \qquad (8)$$

we weight the total squared uncertainty by $w^2(z) = (z/z_{max})^{-7}$ and sum it for prospective objects at n_{depth} evenly spaced depths to form objective function Φ in which the total squared uncertainties for prospective objects at the different depths make approximately equal contributions;

$$\Phi^2 \equiv \sum_{i=1}^{n_{depth}} w^2(z_i)\, \varepsilon^2(z_i) \,/\, n_{depth} \ . \qquad (9)$$

For a multi-receiver system with identical receivers, interchanging receivers leads to a system with identical characteristics. This means that for design of a n_{rec} receivered system, raw object function Φ, considered as a function of receiver coordinates, has at least $n_{rec}!$ global minima. To reduce the number of global minima, a penalty term of form $\Psi \cdot \Phi$ is added to Φ. Numbering receivers from 1 to n_{rec}, Ψ is given a term of the form

$$30 \sum_{i=1}^{n_{rec}-1} max(0, \phi_i - \phi_{i+1}) \cdot min(r_i, r_{i+1}) \ , \qquad (10)$$

to single out the minima of Φ that have receivers ordered with ϕ_i increasing, where ϕ_i and r_i are the angular position in radians and the radius in meters of the i'th receiver. Because of transmitter symmetries, there is commonly an ambiguity as to receiver array orientation: penalty function Ψ is given a second term constraining the receiver at greatest radius to lie at an angular position between -π and -π/2 fixing the array orientation with respect to reflection in x and y axes. An addition term is added to keep receivers within a prescribed region (e.g., inside a horizontal transmitter loop). When individual receiver orientations are allowed to vary, similar terms are added to keep receiver orientations in the upper hemisphere and to keep receiver orientation azimuths between -π and π radians.

Computation of polarizability uncertainties for a test object at some position requires specifying the polarizability of the test object to within a scale factor (Smith and Morrison, 2002) (or determining $\mathbf{M}$ through inversion of data). Each orientation of a non-spherical test object results in a different $\mathbf{M}$, and thus, different uncertainties in its polarizabilities. To avoid the need for multiple orientations of the test object at the control points where ε is evaluated in quantity (9) in many cases we optimize the receiver configurations for spherical targets at the control points.

OPTIMIZATION OF STAND ALONE SYSTEMS

The most comprehensive instruments for determining object polarizability and location would consist of three source coils operated independently to generate source fields in three approximately orthogonal directions and an array of receivers. With sufficient receivers to determine polarizability and position from measurements at a single siting, such a system has the advantage of allowing accurate location and orientation of receivers relative to the transmitter system, eliminating errors that result from uncertainties in relative receiver locations and orientation (e.g., Barrow and Nelson, 2001).

Among the most obvious source coil configurations are a horizontal loop and two vertical loops at right angles with their bottom edges in the plane of the horizontal loop, or, a simple horizontal loop and two figure eight horizontal loops coincident with the horizontal loop but rotated 90^o relative to each other. For both these configurations a limiting factor is the horizontal magnetic field strengths achieved below the system, as the horizontal fields are smaller than the vertical fields at most locations below the coils for loops and currents of identical size. Close to the source, figure eight loops give greater horizontal fields than a vertical loop of the same size, but figure eight loop fields fall off faster with distance, with a vertical loop giving greater horizontal fields by a depth of 0.75 loop widths for loops with a square perimeter. In this study, we adopt the three orthogonal loop configuration, with vertical loops crossed, with their lower edges intersecting at the center of the horizontal loop. To keep transmitters easily maneuverable, we restrict the horizontal transmitter to a 0.75 m x 1 m size, and vertical transmitters to a 1 m x 0.75 m loop and a 0.75 m x 0.75 m loop crossed with lower edges intersecting at the center of the horizontal loop. Each loop is assumed to be given a moment of 180 A-m^2 when transmitting. Receivers are assumed to have a noise level of 2 nT/s when vertical, simulating a noise level observed in an existent commercial transmitter receiver system at 610 μs (Geonics EM-61). For receivers oriented an angle θ from vertical, the noise level is assumed to be $(\cos\theta + 3\sin\theta) \cdot 2$ nT/s simulating the larger noise levels found in off-vertical receivers. Of course, Φ scales with the magnitude of receiver noise, and inversely with the magnitude of transmitter current, so optimal receiver locations are independent of the scale of these.

We minimize $(1+\Psi)\Phi$ with the weighted squared polarizability uncertainties for spherical objects averaged over 20 control positions between 0.2 m and 1.6 m depth directly below the center of the transmitter system, with a sample population size m_{pop} twenty times the number of unknowns. Early experience minimizing $(1+\Psi)\Phi$ allowing receiver positions to vary above the plane of the horizontal transmitter has resulted in receivers negligibly above this level, so in all cases shown, receivers

Number of Receivers	Radius (m)	ϕ (^{o})	Scatter (m)	$\Phi/\sqrt{3}$ (Amp-m^2/T/s)
4	0.702	-114.0	0.17	33432.
unconstrained	0.286	-10.3	0.15	
	0.701	66.2	0.19	
	0.285	169.7	0.13	
4	0.625	-126.9	0.03	34132.
within loop	0.254	-28.3	0.08	
	0.625	53.1	0.05	
	0.246	152.0	0.08	
5	0.879	-159.6	0.19	26741.
unconstrained	0.053	-87.3	0.15	
	0.415	-85.8	0.35	
	0.787	23.4	0.26	
	0.362	135.2	0.14	
5	0.625	-126.9	0.01	28188.
within loop	0.509	-44.0	0.07	
	0.047	-44.0	0.06	
	0.625	53.1	0.03	
	0.624	127.0	0.09	
6	0.854	-122.5	0.28	23425.
unconstrained	0.246	-85.3	0.18	
	0.827	-24.8	0.30	
	0.024	20.3	0.09	
	0.417	50.8	0.27	
	0.775	150.3	0.23	
6	0.625	-126.9	0.02	24548.
within loop	0.550	-47.1	0.07	
	0.042	-31.5	0.05	
	0.625	53.1	0.04	
	0.625	126.9	0.07	
	0.074	134.2	0.06	

Table 1: Receiver positions for optimized stand alone systems with 3 orthogonal loop transmitter system. Receivers vertical. Optimized for spherical objects.

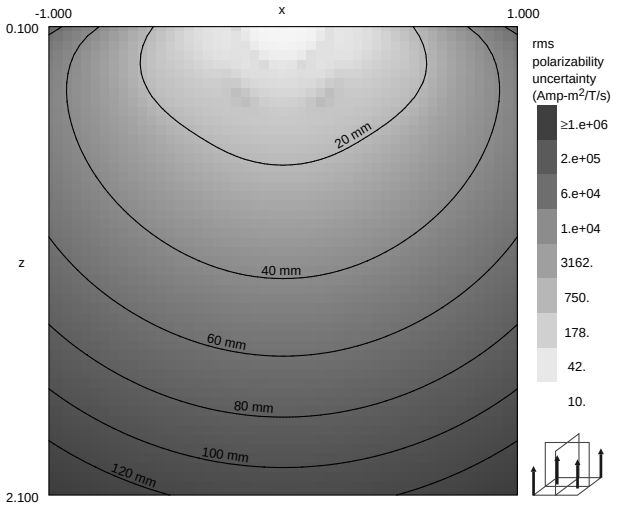

Figure 1: Rms polarizability uncertainty $\varepsilon/\sqrt{3}$ as a function of object position relative to horizontal transmitter loop center, for spheres below optimized 4 receiver array of Table (1) with receivers constrained to lie within the horizontal transmitter loop. Configuration is diagrammed in corner.

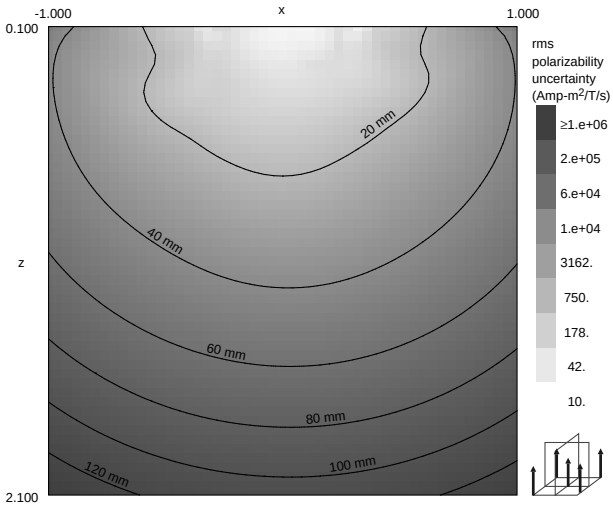

Figure 2: Rms polarizability uncertainty as a function of object position, for spheres below optimized 5 receiver array of Table (1) with receivers constrained to lie within the horizontal transmitter loop.

have been constrained to lie in the plane of the horizontal transmitter loop. For spherical test objects, in our experience minimizing $(1+\Psi)\Phi$ and allowing receiver orientations to vary has resulted in receivers aligned vertically, so in most cases shown, receiver orientations have been fixed at vertical. This reduces the number of unknowns to two per receiver. Results for 4, 5, and 6 receiver systems are given in Table (1), for the case of receivers constrained to be within a radius of 2.6 m ('unconstrained'), and for the case of receivers constrained to lie within the 1.0 x 0.75 m horizontal transmitter loop. For these systems, constraining the receivers to lie within the horizontal transmitter loop increases the object function by less than 6%. Table (1) also lists the root mean square (rms) scatter in receiver position calculated for the best $m_{pop}/2$ sample points at an iteration with the median object function value 10% higher than the minimum value found. This gives an indication of the range of receiver positions that are allowable, but does not indicate how, when one receiver position is altered, the other receiver positions must be adjusted to keep a low object function value.

The receiver arrays listed in Table (1) have been optimized for resolving the polarizability elements for spherical objects below the center of the transmitter array. In Figures (1) and (2), the rms polarizability uncertainty $\varepsilon/\sqrt{3}$ is plotted as a function of object position for test spheres located in cross sections below 4 and 5 receiver arrays. The plots are marked with contours at the polarizability magnitudes (at 610 μs after transmitter shut-off), for spheres of varying diameter. For the 5 receiver system, even at depths near the 0.35m, where lateral gradients in uncertainties are greatest, the minimum is broad laterally suggesting that the instrument can be used on a grid with spacings on the order of 0.6 m laterally, and still result in fairly even coverage. A plot for the 6 receiver system with receivers inside the horizontal loop (not shown) is very similar to Figure (2), with marginally lower uncertainties.

Although the systems of Table (1) were optimized based on polarizability uncertainties that would be obtained when the polarizability matrix $\mathbf{M}$ and equivalent dipole position $\mathbf{r}_o$ are estimated from data for a spherical object, one can evaluate the polarizability uncertainties that would arise for data from other objects. As a magnetic (i.e., ferrous) object becomes long and narrow the largest principal polarizability (eigenvalue of $\mathbf{M}$), corresponding to source magnetic fields aligned with the length

Radius (m)	ϕ (^{o})	Scatter (m)	Declination (^{o})	Azimuth (^{o})	$\Phi/\sqrt{3}$ (Amp-m^2/T/s)
0.318	-157.6	0.02	0.0	—	123585.
0.625	-126.9	0.03	0.0	—	
0.621	-53.6	0.05	89.9	-58.7	
0.318	22.4	0.02	0.0	—	
0.625	53.1	0.03	0.0	—	
0.625	-126.9	0.04	0.0	—	90845.
0.550	-61.5	0.06	90.0	-49.3	
0.330	-22.1	0.04	0.0	—	
0.625	53.1	0.04	0.0	—	
0.550	118.5	0.06	90.0	130.7	
0.330	157.9	0.04	0.0	—	

Table 2: Receiver positions and orientations for optimized stand alone systems with 3 orthogonal loop transmitter system and 5 or 6 receivers. Optimized for elongate objects (1:1:1000 polarizabilities). Symmetry imposed. Receivers constrained to be within horizontal transmitter loop.

of the object, becomes much larger than the other two (e.g., Pasion and Oldenburg, 2001), and the uncertainties in estimated polarizability are dependent on object orientation as well as the ratios of principal polarizabilities. In Figures (3), (4) and (5), rms polarizability uncertainty is plotted as a function of object orientation for systems with 4, 5 and 6 receivers, for an elongate axially symmetric object with a 1:1:1000 ratio of principal polarizabilities one meter below the horizontal transmitter loop center. Only the upper hemisphere of orientations is shown as the lower hemisphere of orientations is the same with azimuths rotated 180^o. The rms polarizability uncertainties for vertical objects (at figure center) are about the same as those for spherical objects at 1 m depth shown in Figures (1) and (2). A curve of orientations with very large uncertainties occurs for the 4 receiver system, and similar curves of orientations with very large uncertainties have been seen in all such plots made for 4 receiver 3 transmitter systems at a single site, for objects with such extreme ratios of principle moments. In the same plot, for the 5 receiver system, the large uncertainties occur for only a few orientations of the elongate object, and are greatly reduced in the plot for the 6 receiver system. In the plots for the 5 and 6 receiver systems, there is a background trend towards lower uncertainties for vertical objects and roughly three times greater uncertainties for horizontal objects. This trend is exacerbated at greater depth; by 1.6m depth (not shown) rms polarizability uncertainties for vertical objects are 7 10^4 and 6 10^4 Amp-m^2/T/s for the 5 and 6 receiver arrays, and are on the order of 30 times larger for horizontal objects.

The polarizability uncertainties for deep horizontal elongate objects can be ameliorated by modifying the objective function to minimize the weighted squared uncertainty for elongate objects in place of spheres. To do this we minimize $(1+\Psi)\Phi$ with the weighted squared polarizability uncertainties for elongate objects averaged over 10 control points between 0.2 m and 1.6 m depth directly below the center of the transmitter system and averaged over 7 equally spaced object orientations at each control point. Three orientations are in the $\hat{\mathbf{x}}$, $\hat{\mathbf{y}}$ and $\hat{\mathbf{z}}$ directions, the others are in the directions of four corners a cube with the coordinate axes going through the face centers. Because of symmetry with respect to inversion in the origin, this covers directions from the 8 corners and 6 face centers of the cube. For simplicity, the test object is given a single non-

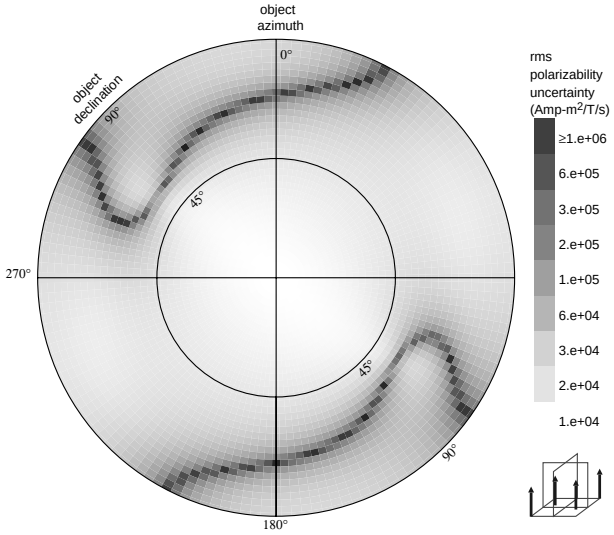

Figure 3: Rms polarizability uncertainty as a function of object orientation (relative to vertical), for an elongate object with principal polarizabilities in a 1:1:1000 ratio, 1 m below 4 receiver array of Figure (1).

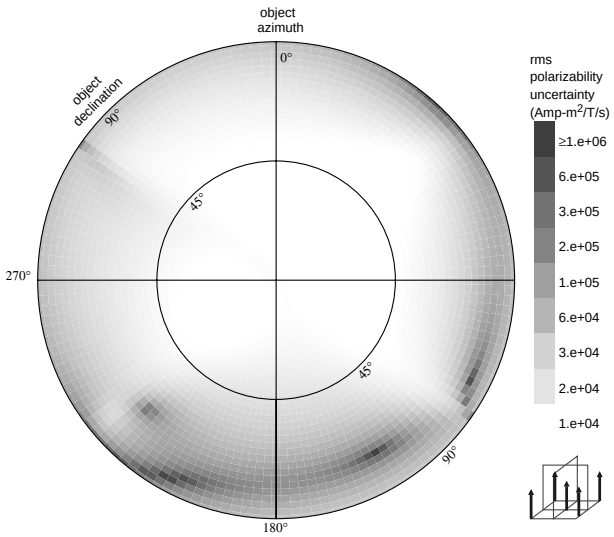

Figure 4: Rms polarizability uncertainty as a function of object orientation, for an elongate object with principal polarizabilities in a 1:1:1000 ratio, 1 m below 5 receiver array of Figure (2).

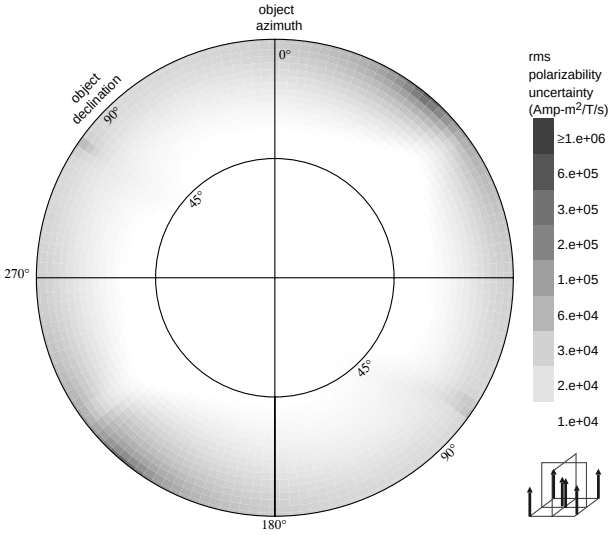

Figure 5: Rms polarizability uncertainty as a function of object orientation, for an elongate object with principal polarizabilities in a 1:1:1000 ratio, 1 m below 6 receiver array of Table (1), with receivers constrained to lie within the horizontal transmitter loop.

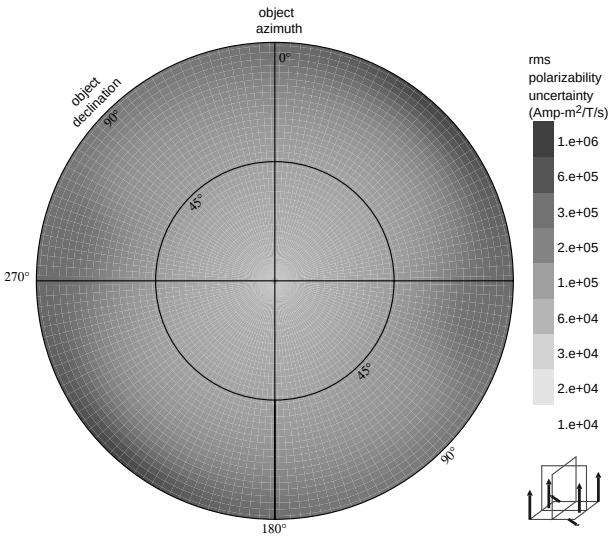

Figure 6: Rms polarizability uncertainty as a function of object orientation, for an elongate object with principal polarizabilities in a 1:1:1000 ratio, 1.6 m below 6 receiver array of Table (2).

zero principal moment. In contrast to the previous minimization in which receiver orientation was held vertical, for elongate objects, a non-vertical receiver orientation may be desirable so it is allowed to vary. To reduce the number of unknown parameters, receivers are constrained to be in symmetric pairs, with the second of each pair reflected through the transmitter system center at equal radius. For an even number of receivers, this keeps the number of unknowns at 2 per receiver. Receiver positions and

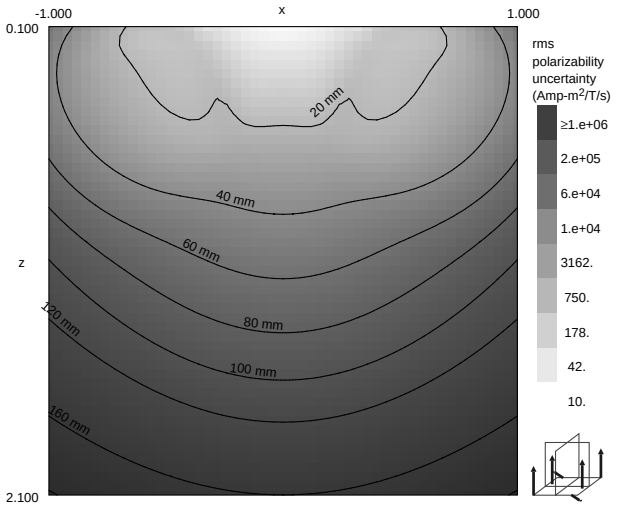

Figure 7: Rms polarizability uncertainty as a function of object position for horizontal elongate object (1:1:1000 polarizability) pointing in the $\hat{\mathbf{y}}$ direction below 6 receiver array of Table (2).

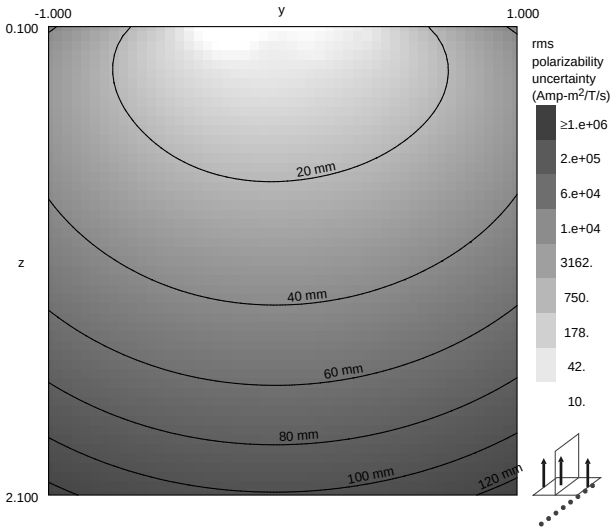

Figure 8: Rms polarizability uncertainty as a function of object position for horizontal elongate object (1:1:1000 polarizability) pointing in the $\hat{\mathbf{y}}$ direction below 6 receiver array of Table (3), used at 8 sites spaced 0.314 m apart along a line at $y = z = 0$ with accurately known locations and orientations.

orientations are given in Table (2) for 5 and 6 receiver arrays. Receiver orientation azimuth has been left blank for receivers that are vertical. Object function values are higher in Table (2) than in Table (1), reflecting greater rms polarizability uncertainties for some orientations of elongate objects.

In Figure (6) rms polarizability uncertainty is plotted as a function of object orientation for the 6 receiver array of Table (2), for an object with a 1:1:1000 ratio of principal polarizabilities 1.6 m below the horizontal transmitter loop center. The rms uncertainty for vertical objects is about the same as was for the 6 receiver array optimized for spheres (of Table 1). For most horizontal orientations the rms uncertainty is substantially smaller than it was for the other array, with few orientations having rms uncertainties near the maximum of 9 10^5 Amp-m^2/T/s. Rms uncertainties for this object at 1.6 m depth below the 5 receiver array of Table (2) (not shown) range from 1. 10^5 Amp-m^2/T/s for vertical objects to 6 10^5 Amp-m^2/T/s for most horizontal orientations, but with two patches of near horizontal orientations with rms uncertainties over 2 10^6 Amp-m^2/T/s. In Figure (7) the rms polarizability uncertainty is plotted as a function of object position for a horizontal 1:1:1000 principal polarizability object pointing in the $\hat{\mathbf{y}}$ direction ($\phi = 90^o$) in cross section below the 6 receiver array of Table (2). Reducing the polarizability ratios to 1:1:40, which is more realistic for UXO at 610 μs, results in an almost identical plot (not shown).

The systems above are capable of estimating $\mathbf{M}$ from measurements with the system at a single site. When data from an object is recorded at more than one siting of a system, estimates of $\mathbf{M}$ can be averaged from adjacent sites to decrease their uncertainties. Provided that system orientation is known, different estimates of $\mathbf{M}$ can be rotated into a common coordinate system and weighted inversely by their rms uncertainties. For such averaging, system site locations need only be known well enough to test whether the equivalent dipole positions from two observations might correspond to a single object.

OPTIMIZATION OF SYSTEMS FOR USE ON LINES OF SITES

If instrument position and orientation are known accurately, measurements from multiple instrument sitings can be combined to estimate an object's polarizability $\mathbf{M}$ directly. This has the advantage of allowing using systems with fewer transmitters and

Δx (m)	Radius (m)	ϕ (^{o})	Scatter (m)	Declination (^{o})	Azimuth (^{o})	$\Phi/\sqrt{3}$ (Amp-m^2/T/s)
0.378	0.265	-137.8	0.05	90.0	-34.7	691755.
0.337	0.368	-110.2	0.09	0.0	—-	40559.
	0.366	68.9	0.09	0.0	—-	
0.314	0.379	-98.0	0.09	0.0	—-	30272.
	0.144	-62.7	0.10	0.0	—-	
	0.378	97.3	0.09	0.0	—-	

Table 3: Site spacing, receiver positions and orientations for 2 orthogonal loop transmitter system operated at 8 sites in a line, with 1 to 3 receivers. Optimized for elongate objects (1:1:1000 polarizabilities). Receivers constrained to be within horizontal transmitter loop.

receivers than in the previous section, but has the disadvantage of requiring accurate system positioning and orientation. In this section, it is assumed that a survey is carried out in lines with relative position and orientation known accurately along sections of survey line, but not between survey lines.

A horizontal loop source operated at a series of sites along a line illuminates objects below that line with magnetic fields oriented in the vertical plane containing the line of sites. Adding a simple vertical loop transmitter in that plane, or a horizontal figure eight loop with one sub-loop on either side of the line, illuminates objects below the line with magnetic fields normal to the vertical plane containing the line of sites. In this study, we adopt the horizontal plus vertical loop configuration, with a 0.75 m wide by 1 m long horizontal loop and a 1 m long by 0.75 m high vertical loop with lower edge through the horizontal loop center. The loops are oriented lengthwise in the direction of the siting line. Transmitters and receivers are assumed to have the same moments and noise levels as in the previous section.

For simplicity we restrict our attention to using data from 8 sites along a survey line, with the intersite spacing as a free parameter. As the rms polarizability uncertainties for elongate objects tend to be larger than for spheres, we minimize $(1+\Psi)\Phi$ with the weighted squared polarizability uncertainties for elongate objects (1:1:1000 polarizability) averaged over 10 control points between 0.2 m and 1.6 m depth below the middle of the survey line segment, and averaged over 7 equally spaced object orientations at each control point. Results for 1, 2, and 3 receiver arrays are given in Table (3). Receiver orientation was allowed to vary. Receiver orientation azimuth has been left blank for vertical receivers. The improvements in object function going from 1 to 3 receivers are better than the $1/\sqrt{n_{rec}}$ improvement to be expected solely from an increase in the number of data. The two and three receiver arrays operated on 8 sites result have quite good angular coverage. For example, at 1.6m depth below the line segment center, the 3 receiver array has a minimum rms moment uncertainty of 4.6 10^4 Amp-m^2/T/s for horizontal elongate objects oriented normal to the line, and a maximum of 1.4 10^5 Amp-m^2/T/s for horizontal elongate objects oriented parallel to the line. Rms polarizability uncertainty for 1:1:1000 polarizability objects oriented parallel to the survey line is plotted as function of position in cross section through the segment center in Figure (8), for the 3 receiver system. Of course, the three transmitter systems of Table (2) also can be used with data from more than one site, giving lower uncertainties (not shown) than the two transmitter three receiver system uncertainties shown here.

Δx (m)	Δy (m)	Radius (m)	ϕ (^{o})	Scatter (m)	Declination (^{o})	$\Phi/\sqrt{3}$ (Amp-m^2/T/s)
0.443	0.417	0.211	-128.3	0.08	0.0	58923.
0.511	0.456	0.587	-140.3	0.06	0.0	24729.
		0.161	61.1	0.08	0.0	
0.528	0.524	0.592	-140.7	0.07	0.0	18627.
		0.000	22.7	0.17	0.0	
		0.586	39.8	0.13	0.0	

Table 4: Site spacing, receiver positions and orientations for horizontal loop transmitter operated at 16 sites on a grid, with 1 to 3 receivers. Optimized for elongate objects (1:1:1000 polarizabilities). Receivers constrained to be within horizontal transmitter loop.

OPTIMIZATION OF SYSTEMS FOR USE ON A GRID

A horizontal loop moved about a two-dimensional surface can illuminate any point beneath the surface with a magnetic field in any arbitrary direction, so, in principle, only one source is needed for an instrument operated on a two dimensional grid. We restrict our attention to data from a 4 x 4 grid sub-section centered over an object. We assume a 0.75 m wide by 1 m long horizontal loop transmitter with a 180 Amp-m^2 moment, sited on a rectangular grid with instrument position and orientation known accurately. We minimize $(1+\Psi)\Phi$ with the weighted squared polarizability uncertainties for elongate objects (1:1:1000 polarizability) averaged over 10 control points between 0.2 m and 1.6 m depth below the middle of the grid sub-section and averaged over 7 equally spaced object orientations at each control point. Results for 1, 2, and 3 receiver arrays are given in Table (4). Receiver orientation was allowed to vary. Receiver orientation azimuth has been omitted as all receivers are vertical. Increasing the number of receivers to four (not shown) improves the object function only marginally better than the improvement expected for an increased number of data. The lower object function values reflect lower rms polarizability uncertainties at all depths (not shown) compared to the results of the previous two sections. However, to achieve these results, system location and orientation must be accurately known at each site.

EFFECTS OF SYSTEM LOCATION ERRORS

The results of the previous two sections require accurate instrument (relative) locations and orientations. For any particular system and object, one can estimate the effect of instrument location errors by Monte Carlo methods: adding artificial noise to synthetic data and adding random mislocations to the system coordinates at each site, inverting for object polarizabilities and location, and repeating to develop statistics. In Figure (9), rms polarizability errors are plotted as a function of system location error for three systems from Tables (2), (3), and (4), for a horizontal 22mm 1:8 aspect ratio ferrous shell modelled as a magnetic conducting prolate spheriod (7.0 10^3: 7.0 10^3: 2.6 10^5 Amp-m^2/T/s principal polarizabilities at 610 μs). In the simulations to produce this figure, Gaussian noise was added to the system x, y and z coordinates at each site and the abscissa site location uncertainties are total location uncertainty $(\sigma_x^2+\sigma_y^2+\sigma_z^2)^{1/2}$. Results from the 3 transmitter 6 receiver system at a single site are unaffected by instrument location errors. Results from the other two systems are strongly affected by instrument location errors, and require instrument lo-

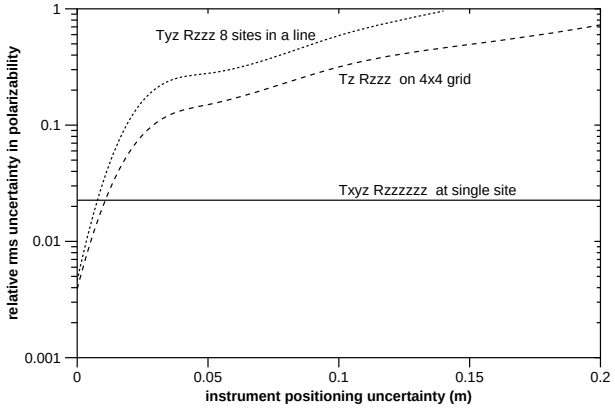

Figure 9: Relative rms polarizability uncertainty as a function of instrument location error, for a horizontal 22 mm 8:1 aspect ratio shell at 0.75 m depth at 610 μs after transmitter shut-off. (Horizontal) for a 3 transmitter 6 vertical component receiver of Table (2) at single site. (Dashed) for a 2 transmitter 3 vertical component receiver system of Table (3) at 8 sites in a line. (Solid) for a horizontal loop transmitter three vertical component receiver system of Table (4) on a 4x4 grid.

cation errors as small as 1 cm to give results comparable to the single site system. This is smaller than typical relative global positioning system errors of 2.5 cm currently available.

CONCLUSION

A weighted rms average of polarizability uncertainties for objects at a series of depths below a system is an objective measure of the discrimination capability of a system. For chosen transmitter configurations, we have found receiver configurations minimizing the polarizability uncertainty using the empirical distribution evolutionary algorithm. Three transmitter, 5 or 6 receiver systems optimized for use at a single site have the advantage that their estimates of object polarizabilities and relative position are unaffected by errors in instrument location and orientation. Systems used on a grid or line of accurately known locations have the advantage of only needing one or two transmitters, but polarizability estimates from them are strongly degraded when contaminated with small instrument location errors.

ACKNOWLEDGEMENT

This work was supported by the US Department of the Army contract No. W74RDV93447299, under the auspices of the Strategic Environmental Research and Development Program (SERDP).

REFERENCES

C. E. Baum, “Low frequency near-field magnetic scattering from highly conducting, but not perfectly conducting bodies,”in C. E. Baum, Ed., *Detection and Identification of Visually Obscured Targets*, Philadelphia: Taylor et Francis, ch. 6, pp. 163-217, 1999.

B. J. Barrow, and H. H. Nelson, “Effects of positioning error on inverting EMI data for UXO discrimination using the MTADS platform,” in *Proceedings of UXO Forum* 2001.

T. H. Bell, B. J. Barrow, and J. T. Miller, “Subsurface discrimination using electromagnetic induction sensors,”*IEEE Trans. Geosci. Remote Sensing,* vol. 39, no. 6, pp. 1286-1293. June 2001.

K. Deb, *Multi-Objective Optimization using Evolutionary Algorithms,* New York: John Wiley et Sons, Ltd., ch. 4, pp. 81-169, 2001.

N. Khadr, B. J. Barrow, T. H. Bell, and H. H. Nelson, “Target shape classification using electromagnetic induction sensor data,” in *Proceedings of UXO Forum* 1998.

L. R. Pasion and D. W. Oldenburg, “Locating and determining dimensionality of UXOs using time domain electromagnetic fields,” *Journal of Environmental and Engineering Geophysics,* vol. 6, no. 2, pp. 91-102, June 2001.

W. H. Press, B. P. Flannery, S. A. Teukolsky, and W. T. Vetterling, *Numerical Recipes, the Art of Scientific Computing.* Cambridge: Cambridge University Press, 1986.

J. T. Smith and H. F. Morrison, “Estimating equivalent dipole polarizabilities for the inductive response of isolated conductive bodies,” *IEEE Trans. Geosci. Remote Sensing,* 2003 (in press).

J. T. Smith and H. F. Morrison, and A. Becker, “Resolution Depths for Some Transmitter Receiver Con-

figurations," *IEEE Trans. Geosci. Remote Sensing*, 2003 (in press).

T. Smith, W. Allan, and A. Schultz, "Inversion of waveform data using an empirical distribution evolutionary algorithm," *Eos*, vol. 75, no. 44, p. 457. December 1994.